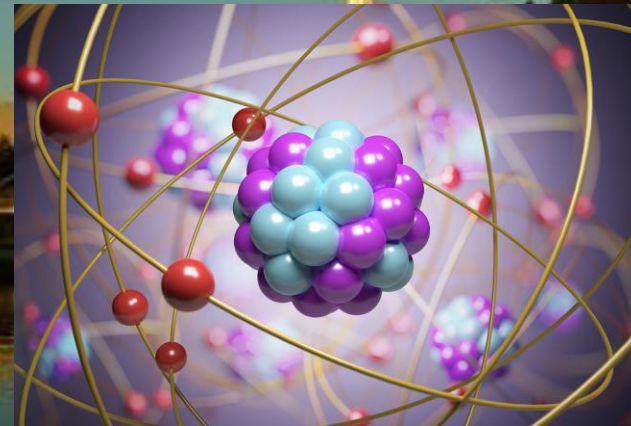


When Axion Cosmology meets the Subaru HSC data

arXiv:2109.13153 [hep-ph]

PARTICLE PHYSICS DAY 2021



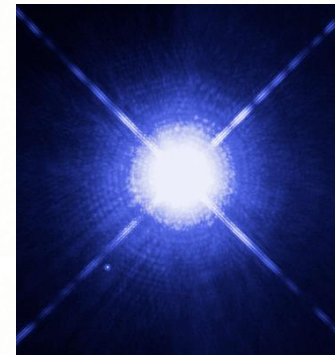
Enrico D. Schiappacasse

University of Jyväskylä & Helsinki Institute of Physics

(with the collaboration of Tsutomu T. Yanagida)

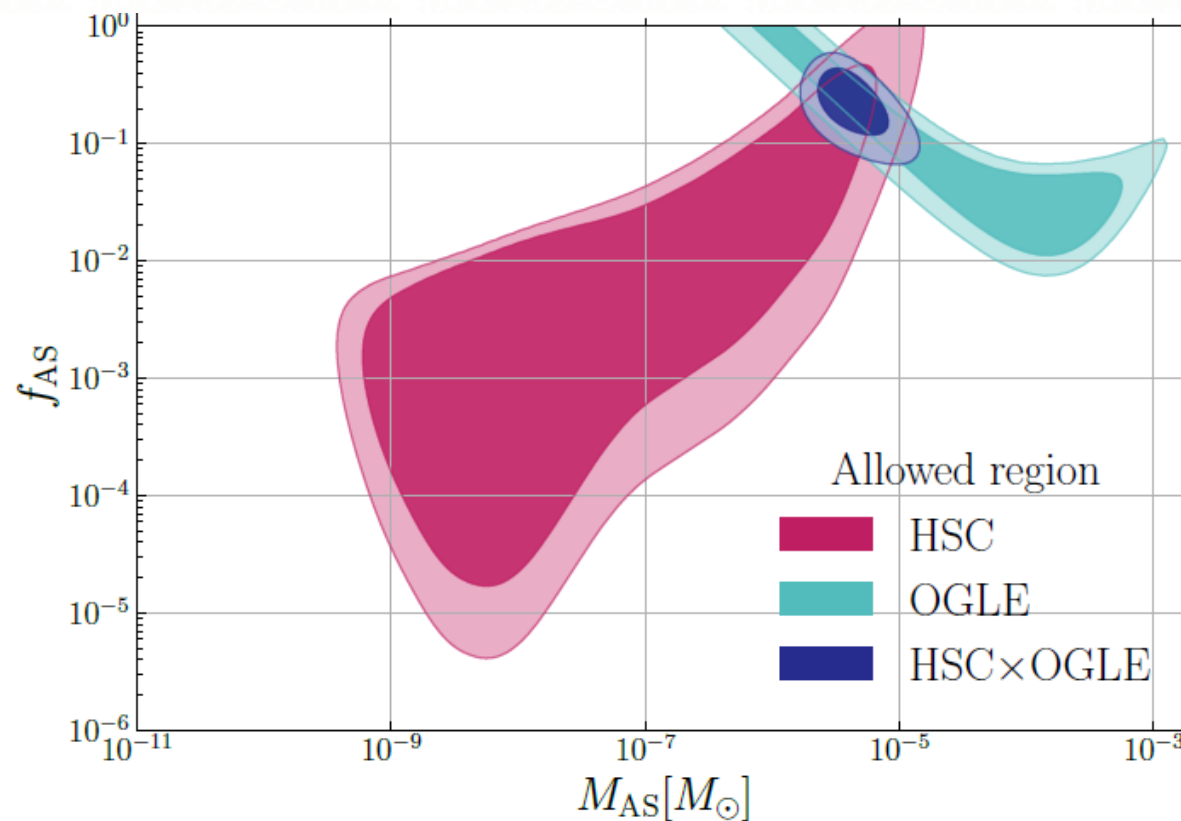
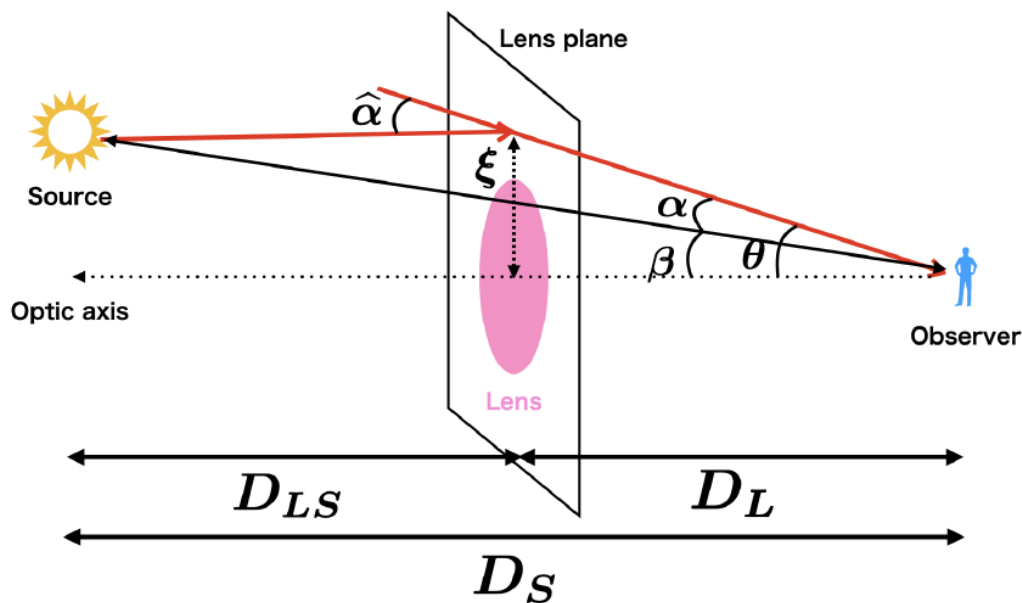
Main question

Can QCD axion stars explain Subaru HSC data?



Gravitational Microlensing Setup

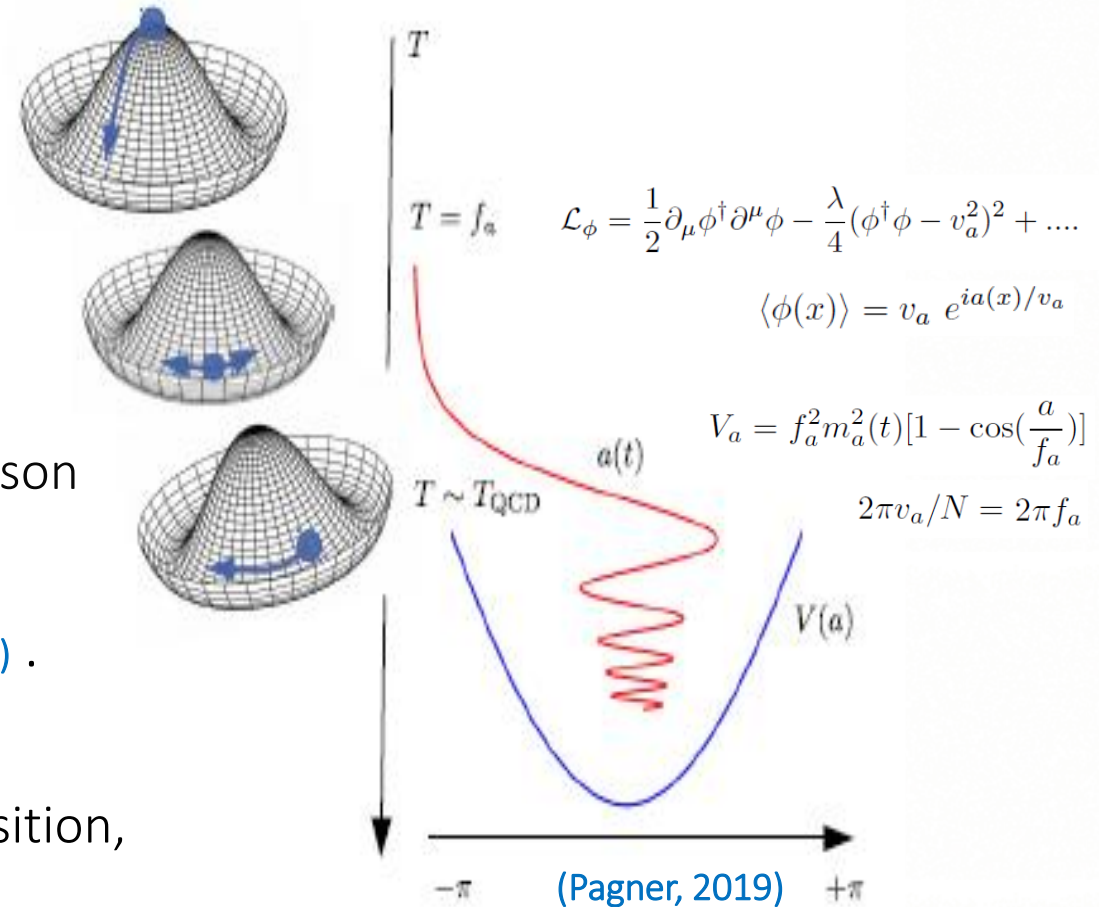
A geometrical setup of the gravitational lensing event is shown. A light ray (the red color line) is deflected by the lens (the pink colored circle) and reaches to the observer (the blue colored human).



(Sugiyama, Takada, and Kusenko, 2021)

QCD-Axion in a nutshell

- A wide range of astrophysical observations are well explained by including **cold dark matter (CDM)** (Peebles, 2015).
- A popular dark matter candidate is the **QCD axion**: PG-boson associated with SSB of $U(1)_{PQ}$, which was introduced as a possible solution of the strong CP problem (Peccei and Quinn, 1977).
- The axion field **acquires a mass** after the QCD phase transition, and then begin to act as a form of **CDM** (Preskill et al. 1983).
- Extensively axion searching



- Ground based experiments as ADMX (Asztalo et al. 2010)
- FRB and axion miniclusters (Tkachev 2015)
- Transient radio emission from axion photon conversion during neutron star-ultracompact minihalo encounters (Nurmi, Schiappacasse, Yanagida, 2021)

Axion Stars

- In the effective theory for axions, they can be described by a real scalar field $\phi(x, t)$ with a small potential $V(\phi)$ coming from **nonperturbative QCD effects**:

$$\mathcal{L} = \sqrt{-g} \left[\frac{R}{16\pi G_N} + g^{\mu\nu} \nabla_\mu \phi \nabla_\nu \phi - V(\phi) \right]$$

$$V(\phi) = \frac{1}{2} m_\phi^2 \phi^2 + \frac{\lambda}{4!} \phi^4 + \mathcal{O}(\phi^6)$$

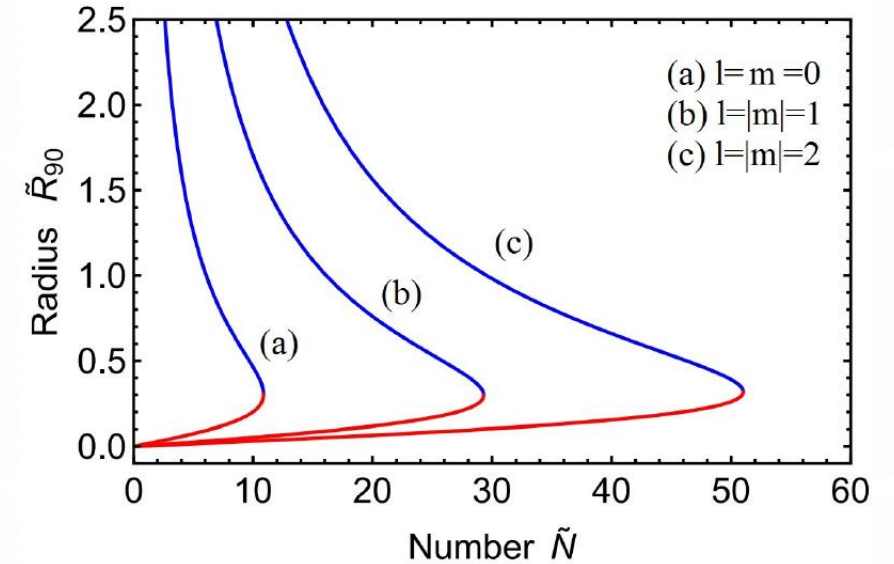
Nonrelativistic approximation

$$\phi(x, t) = \frac{1}{\sqrt{2m_\phi}} \left[e^{-im_\phi t} \psi(x, t) + e^{im_\phi t} \psi^*(x, t) \right]$$

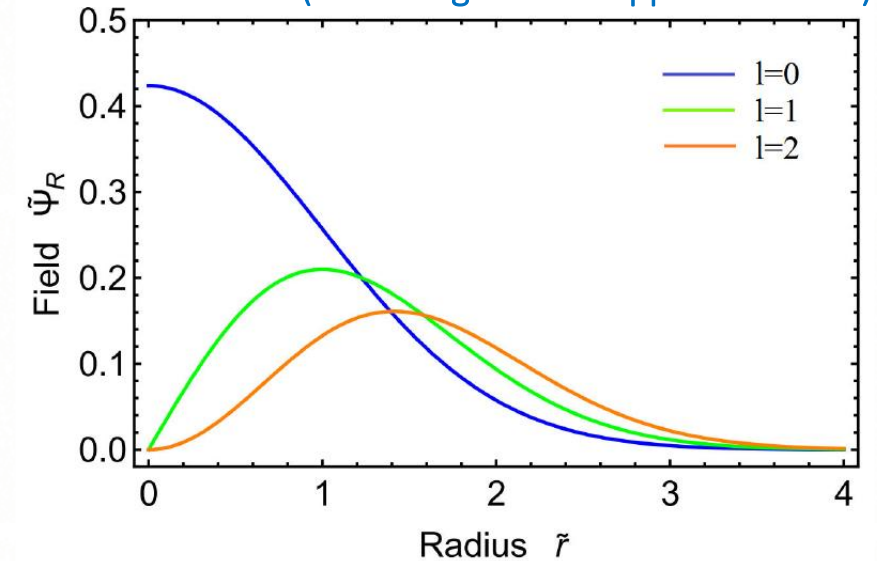
Axion stars are ground state (or higher eigenstates) solutions of the Schrodinger-Poisson equation

$$i\dot{\tilde{\psi}} = -\frac{1}{2} \tilde{\nabla}^2 \tilde{\psi} + \tilde{\psi} \tilde{\phi}_N - \frac{\tilde{\psi}^* \tilde{\psi}^2}{8},$$

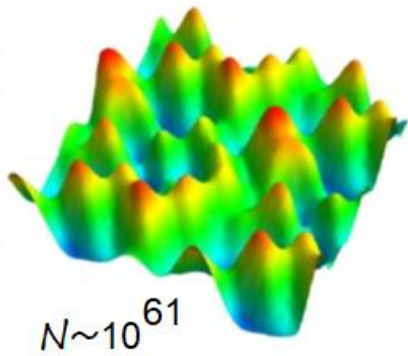
$$\tilde{\nabla}^2 \tilde{\phi}_N = 4\pi |\tilde{\psi}|^2$$



(Hertzberg and Schiappacasse 2018)



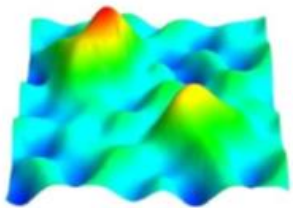
- If the PQ symmetry is broken after inflation, large amplitude axion field fluctuations and topological defects are found on size scales of order the horizon at the time of the SSB.



Number of axion within a typical correlation length in the early Universe



$M \sim 10^{-11} M_{\text{sun}}$
 $N \sim 10^{60}$



(Guth, M.H., Prescod-Weinstein, 2015)

$$M_{\star} \approx 1.2 \times 10^{-11} M_{\odot} \times \alpha \left(\frac{10^{-5} \text{ eV}}{m_a} \right) \left(\frac{F_a}{6 \times 10^{11} \text{ GeV}} \right) \left(\frac{0.3}{\gamma} \right)^{1/2}$$

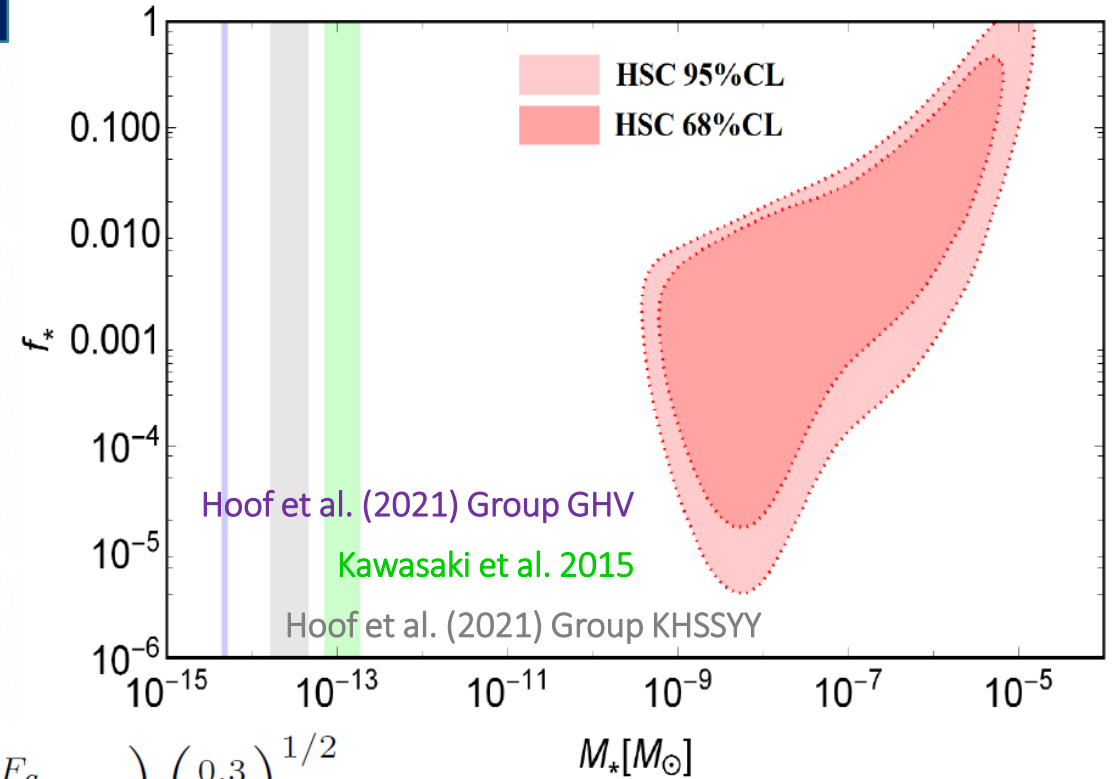
$$R_{\star}^{90} \approx 78 \text{ km} \left(\frac{1 + \sqrt{1 - \alpha^2}}{\alpha} \right) \left(\frac{10^{-5} \text{ eV}}{m_a} \right) \left(\frac{6 \times 10^{11} \text{ GeV}}{F_a} \right) \left(\frac{\gamma}{0.3} \right)^{1/2}$$

$$M_{\star, \text{max}} \propto l^{3/2} / (\ln l)^{1/4}$$

$$R_{\star, \text{min}} \propto l^{1/2} / (\ln l)^{1/4}$$

QCD-AXION

$$m_a = 6 \mu\text{eV} \left(\frac{10^{12} \text{ GeV}}{f_a} \right)$$



For angular momentum $l = |m| > \mathcal{O}(10^2)$, we will have $M_{\star, \text{max}} > \mathcal{O}(10^{-10}) M_{\odot}$

¿Does it possible? (Dmitriev et al. 2021; Hertzberg et al. 2020)

Nucleation in axion miniclusters

- The large axion field fluctuations produced by the SSB remain smooth up to scales of order the horizon size at the time when the axion acquires its mass.
- Density perturbations may grow under gravity as usual to collapse into gravitationally bound DM substructures known as miniclusters at around matter-radiation equality.
- Because of the randomness of the initial axion overdensity fluctuations and the subsequent evolution of the minicluster halo mass function via hierarchical structure formation during matter domination

$$\rightarrow 10^{-19} M_{\odot} \lesssim M_{AMC} \lesssim 10^{-5} M_{\odot}$$

$$R_{\star} = 1.5 \text{ km} \left(\frac{10^{-10} M_{\odot}}{M_{\star}} \right) \left(\frac{10^{-5} \text{ eV}}{m_a} \right)^2$$

$$M_{\star} = 1.4 \times 10^{-16} M_{\odot} (1 + z_{\star})^{1/2} \times \left(\frac{\zeta(z_{\star})}{\zeta(0)} \right)^{1/6} \left(\frac{10^{-5} \text{ eV}}{m_a} \right) \left(\frac{M_{AMC}}{10^{-10} M_{\odot}} \right)^{1/3}$$

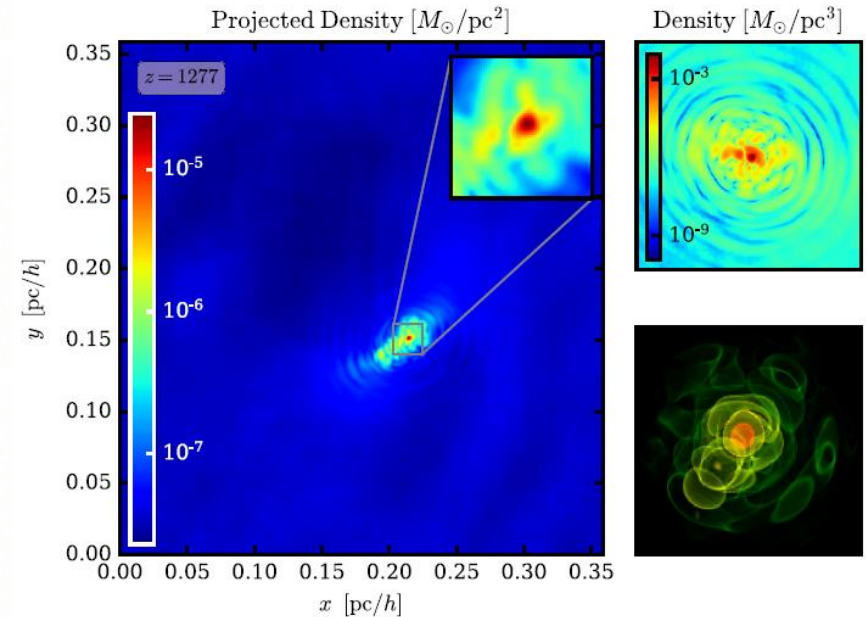
Axion Stars Nucleation

Formation and mass growth of axion stars in axion miniclusters

Benedikt Eggemeier^{1,*} and Jens C. Niemeyer^{1,2}

¹Institut für Astrophysik, Universität Göttingen, Germany

²Department of Physics, University of Auckland, Private Bag 92019, Auckland, New Zealand



The density profile of the incoherent halo decay as $r^{-9/4}$

The axion stars form roughly during **a few free-fall times** after the collapse of the minicluster.

Axion stars are surrounded by pronounced **density waves**.

Axion Stars Nucleation in axion minihalos around PBHs

- Since PBHs are local overdensities in the DM distribution, they act as seeds for DM structure formation.
- Evolution of a DM spherical layer around a central PBH (theory of spherical gravitational collapse)



$$\frac{d^2r}{dt^2} = -\frac{G_N(M_{PBH} + DM)}{r^2} - \frac{8\pi G_N \rho_r r}{3} + \frac{8\pi G_N \rho_\Lambda r}{3}$$

$$M_{\text{halo}}(z) = 3 \left(\frac{1000}{1+z} \right) M_{\text{PBH}},$$

$$R_{\text{halo}}(z) = 0.019 \text{ pc} \left(\frac{M_{\text{halo}}}{M_\odot} \right)^{1/3} \left(\frac{1000}{1+z} \right).$$

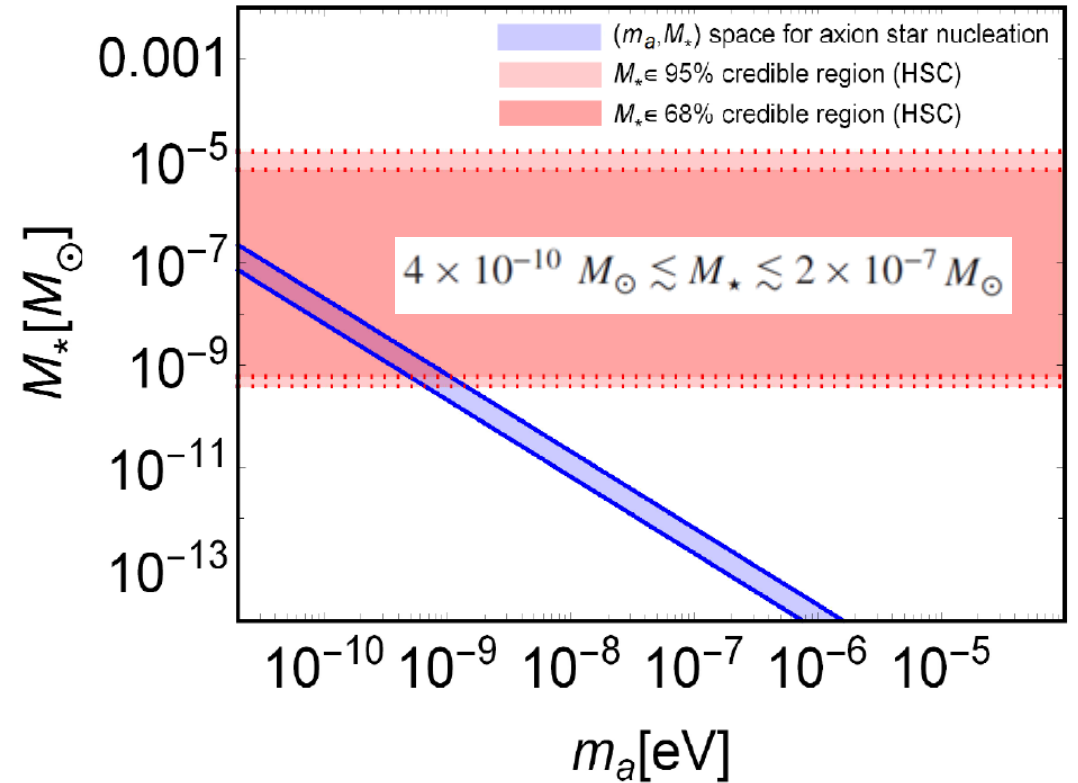
(Mack, Ostriker and Ricotti, 2007)

(Levkov, Panin and Tkackev, 2018)

$$\tau_{gr} \sim m_a^3 v_a^6 \rho_{\text{halo}}^{-2}$$

- The kinetic formation of axion stars in dark mini-halos depends on the halo energy density, axion mass and velocity

(Schiappacasse and Yanagida 2021)



$$R_E = \sqrt{\frac{4G_N M D_L D_{LS}}{c^2 D_S}} = 4.3 \times 10^8 \text{ km} \left(\frac{M}{M_\odot} \right)^{1/2} \left(\frac{D_S}{\text{kpc}} \right)^{1/2}$$



$$35 \lesssim R_\star / R_E \lesssim 80$$

Magnification is shutted-off

1. The known mechanisms for QCD axion clump formation in the pre- and postinflationary PQ symmetry-breaking scenario are not able to explain the microlensing event reported by the Subaru HSC observation.
2. In the postinflationary scenario, the needed mass for axion stars is larger than the allowed maximum mass for a stable configuration. Since the QCD axion mass is strictly bounded from below due to the axion decay of topological defects, the typical axion star masses are $M_* \lesssim 10^{-13} M_\odot$.
3. In the preinflationary scenario, the nucleation of axionclumps within axion self-similar minihalos around PBHs produce axion stars within the lightest part of the credible region associated with HSC data. However, such stars are very diluted having radii larger than their associated Einstein radius.
4. Axion clumps with sufficiently heavy masses to explain the Subaru HSC observation could be formed in some nonstandard cosmologies, but their nucleation is highly model dependent.



FURTHER DISCUSSION

AXION FIELD THEORY

- In the effective theory for axions, they can be described by a real scalar field $\phi(x, t)$ with a small potential $V(\phi)$ coming from **nonperturbative QCD effects**:

$$\mathcal{L} = \sqrt{-g} \left[\frac{R}{16\pi G_N} + g^{\mu\nu} \nabla_\mu \phi \nabla_\nu \phi - V(\phi) \right]$$

- Expanding around the CP preserving vacuum: $V(\phi) = \frac{1}{2} m_\phi^2 \phi^2 + \frac{\lambda}{4!} \phi^4 + \mathcal{O}(\phi^6)$

$$\lambda = -\gamma \frac{m_\phi^2}{F_a^2}$$

$$\begin{aligned} \gamma = 1: \quad & V(\phi) = m_\phi^2 f_a^2 [1 - \cos(\phi/f_a)] \\ \gamma = 1 - 3m_u m_d / (m_u + m_d)^2 \approx 0.3 & \text{ (Grilli et al., 2016)} \end{aligned}$$

- For the **standard QCD axion** (Weinberg, 1978):

$$m_\phi(m_{u,d,\pi}, f_\pi, f_a) \simeq 10^{-5} \text{eV} \left(\frac{6 \cdot 10^{11} \text{GeV}}{F_a} \right)$$

- In the non-relativistic regime we can rewrite the real axion field in terms of a complex Schrodinger field ψ (slowly varying)

$$\phi(\mathbf{x}, t) = \frac{1}{\sqrt{2m_\phi}} [e^{-im_\phi t} \psi(\mathbf{x}, t) + e^{im_\phi t} \psi^*(\mathbf{x}, t)]$$

- Using the weak field approximation, we obtain the non-relativistic lagrangian for ψ as

$$\mathcal{L}_{nr} = \frac{i}{2} (\dot{\psi}\psi^* - \psi\dot{\psi}^*) - \frac{1}{2m_\phi} \nabla\psi^* \cdot \nabla\psi - \gamma \frac{\psi^{*2}\psi^2}{16F_a^2} - m_\phi \psi^* \psi \phi_N(\psi^*, \psi)$$

$$\phi_N = -G_N m_\phi \int d^3x' \frac{|\psi(\mathbf{x}')|^2}{|\mathbf{x} - \mathbf{x}'|} \text{ is Newtonian potential}$$

- By performing Legendre Transformations, the dynamics of ψ is given by the standard non-relativistic Hamiltonian:

$$H_{nr} = H_{kin} + H_{int} + H_{grav}$$

$$H_{kin} = \frac{1}{2m_\phi} \int d^3x \nabla\psi^* \cdot \nabla\psi, \quad H_{int} = \frac{\lambda}{16m_\phi^2} \int d^3x \psi^{*2} \psi^2,$$

- H_{nr} carries a global $U(1)$ symmetry $\psi \rightarrow \psi e^{i\theta}$ associated with a conserved particle number $N = \int d^3x \psi^*(\mathbf{x})\psi(\mathbf{x})$

$$H_{grav} = -\frac{Gm_\phi^2}{2} \int d^3x \int d^3x' \frac{\psi^*(\mathbf{x})\psi^*(\mathbf{x}')\psi(\mathbf{x})\psi(\mathbf{x}')}{|\mathbf{x} - \mathbf{x}'|}$$

(Guth, Hertzberg, and Prescod-Weinstein, 2015; Schiappacasse and Hertzberg, 2017)

- From Hamilton equation  Equation of motion of the field in the non-relativistic regime

$$i\dot{\tilde{\psi}} = -\frac{1}{2}\tilde{\nabla}^2\tilde{\psi} + \tilde{\psi}\tilde{\phi}_N - \frac{\tilde{\psi}^*\tilde{\psi}^2}{8},$$

$$\tilde{\nabla}^2\tilde{\phi}_N = 4\pi|\tilde{\psi}|^2$$

$\tilde{\phi}_N = \tilde{\phi}_N(\tilde{\psi}^*, \tilde{\psi})$
is the dimensionless (non-dynamical)
Newtonian potential

- All quantities have been re-scaled for numerical purposes as

$$x = \left(\frac{m_{pl}\gamma^{1/2}}{m_\phi F_a}\right)\tilde{x}, \quad t = \left(\frac{m_{pl}^2\gamma}{m_\phi F_a^2}\right)\tilde{t}$$

$$\psi = \left(\frac{m_\phi^{1/2}F_a^2}{m_{pl}\gamma}\right)\tilde{\psi}, \quad \phi_N = \left(\frac{F_a^2}{m_{pl}^2\gamma}\right)\tilde{\phi}_N$$

SPHERICALLY SYMMETRIC CLUMP CONDENSATES

$\Psi(r)$ describes the radial profile
 μ describes the correction to the frequency

- The **true BEC ground state** is guaranteed to be spherically symmetric: $\psi(r, t) = \Psi(r)e^{-i\mu t}$
- The time independent field equation for a spherically symmetric eigenstate is

$$V_{nr} = -\gamma \frac{\Psi^4}{16F_a^2}$$

$$\mu\Psi = -\frac{1}{2m} \left(\Psi'' + \frac{2}{r} \Psi' \right) - 4\pi G_N m^2 \Psi \int_0^\infty dr' r'^2 \frac{\Psi(r')^2}{r_{>}} + \frac{1}{2} \frac{\partial V_{nr}}{\partial \Psi}$$

Near field region ($r \rightarrow 0$): Corrections from self-interactions become important. There are no known full analytic solutions.

Far field region ($r \rightarrow \infty$)

- $\Psi \rightarrow 0$ as $r \rightarrow \infty$
- At large distances we may ignore the self-interactions
- In the gravitational term we may replace $r_{>} \rightarrow r$ in the far region.
- Identical to the structure of the **time independent Schrödinger equation** for the hydrogen atom under replacement $Gm^2N \rightarrow e^2$

$$\mu\Psi = -\frac{1}{2m} \left(\Psi'' + \frac{2}{r} \Psi' \right) - \frac{G_N m^2 N_*}{r} \Psi \quad \text{(far region)}$$

$$\Psi_R(r) = \sqrt{\frac{N_*}{\pi R^3}} e^{-r/R},$$

$$\Psi_R(r) = \sqrt{\frac{3N_*}{\pi^3 R^3}} \operatorname{sech}(r/R),$$

$$\Psi_R(r) = \sqrt{\frac{N_*}{7\pi R^3}} (1 + r/R) e^{-r/R}.$$

Stable Branch for axion clumps

(Schiappacasse and Hertzberg 2018)

Any localized ansatz of a single parameter R

$$\tilde{H}(\tilde{R}) = a \frac{\tilde{N}_*}{\tilde{R}^2} - b \frac{\tilde{N}_*^2}{\tilde{R}} - c \frac{\tilde{N}_*^2}{\tilde{R}^3}$$

$$N_* = 4\pi \int_0^\infty |\psi(r, t)|^2 r^2 dr$$

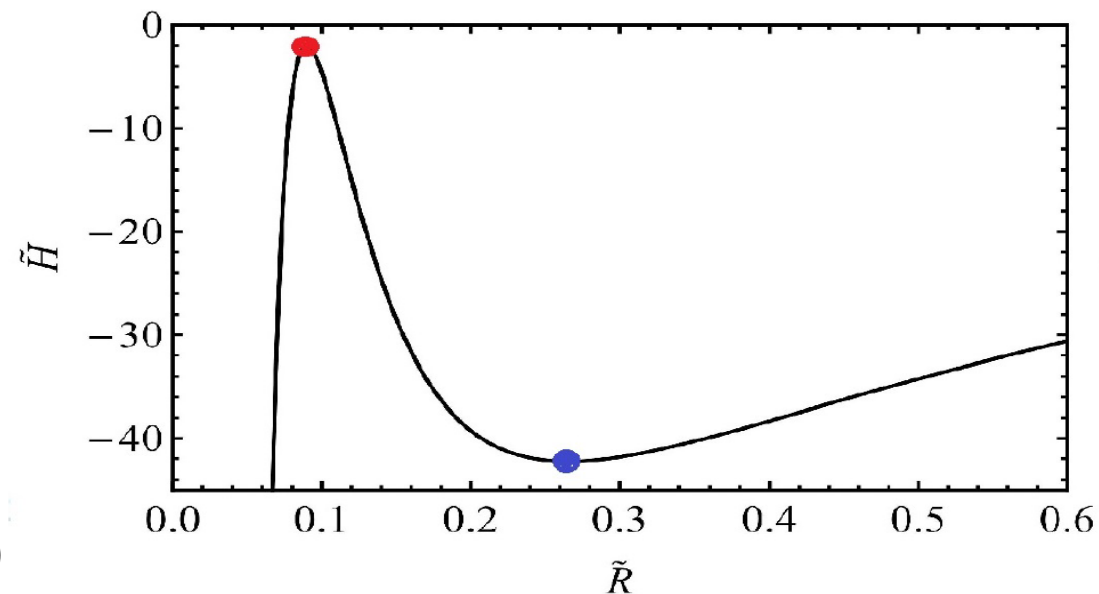
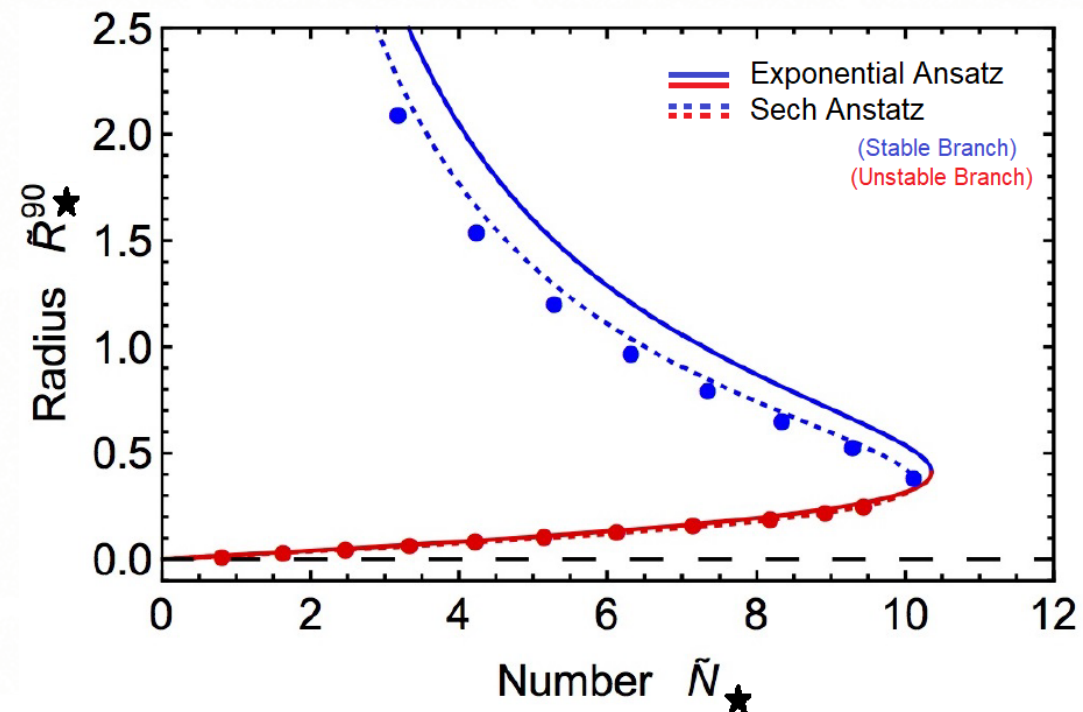
- $H = \left(\frac{F_a^3}{m_{pl} m_\phi \gamma^{3/2}} \right) \tilde{H}$
- $R = \left(\frac{m_{pl} \gamma^{1/2}}{m_\phi F_a} \right) \tilde{R}$
- $N_* = \left(\frac{m_{pl} F_a}{m_\phi^2 \gamma^{1/2}} \right) \tilde{N}_*$
- $M_* = m_\phi N_*$

R is the effective radius of the solution (variational parameter)

- Apply $\frac{d\tilde{H}}{d\tilde{R}} = 0$ to obtain conditions for stationary solutions
- For any value of $(\tilde{a}, \tilde{b}, \tilde{c})$ there are two branches of solutions

$$\tilde{R} = \frac{a \pm \sqrt{a^2 - 3bc\tilde{N}_*^2}}{b\tilde{N}_*}$$

State of minimum energy at fixed \tilde{N}_* (spherically symmetry)



- We numerically solve the full equation of motion of the axion field within the spherically symmetric ansatz:

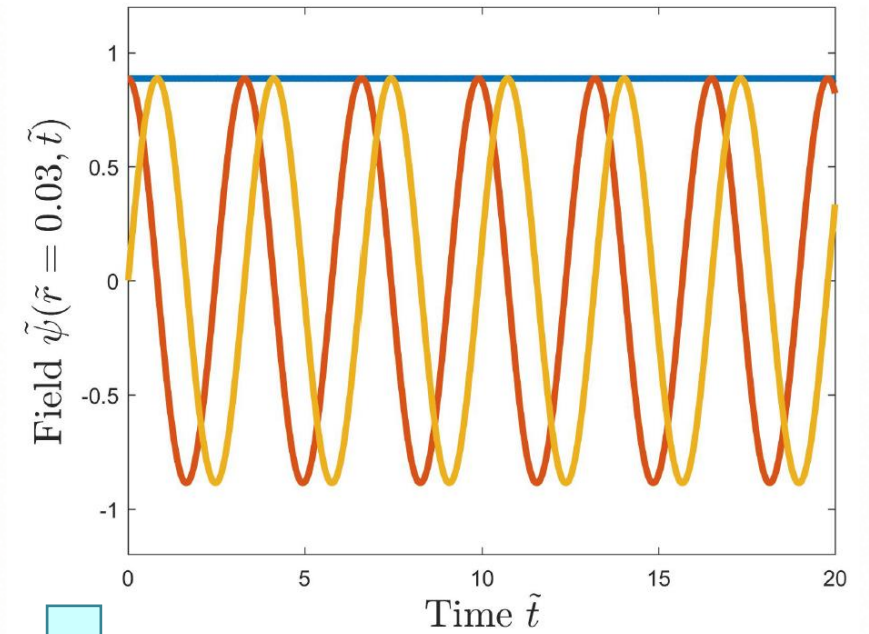
$$i\dot{\tilde{\psi}} = -\frac{1}{2} \frac{\partial^2}{\partial \tilde{r}^2} (\tilde{r}\tilde{\psi}) + \tilde{\psi}\tilde{\phi}_N - \frac{\tilde{\psi}^*\tilde{\psi}^2}{8}$$

$$\frac{1}{\tilde{r}} \frac{\partial^2}{\partial \tilde{r}^2} (\tilde{r}\tilde{\phi}_N) = 4\pi|\tilde{\psi}|^2$$

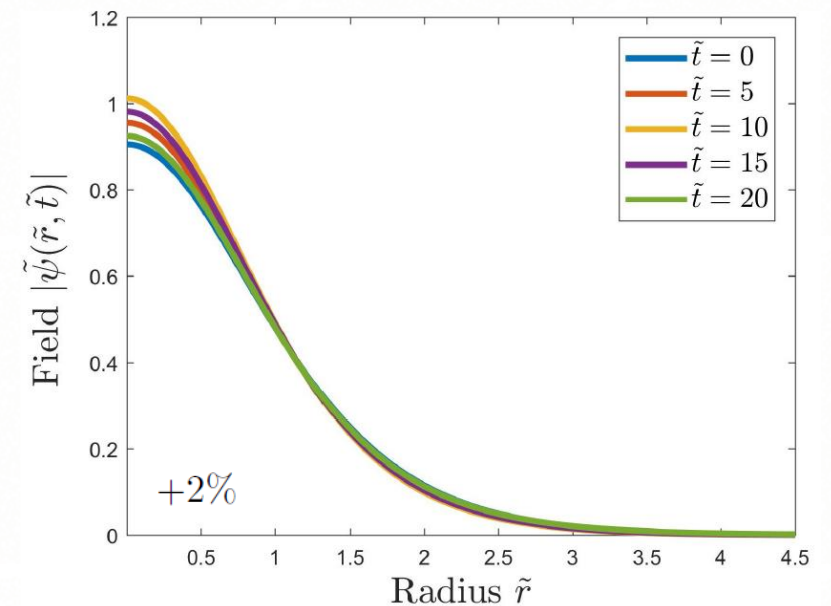
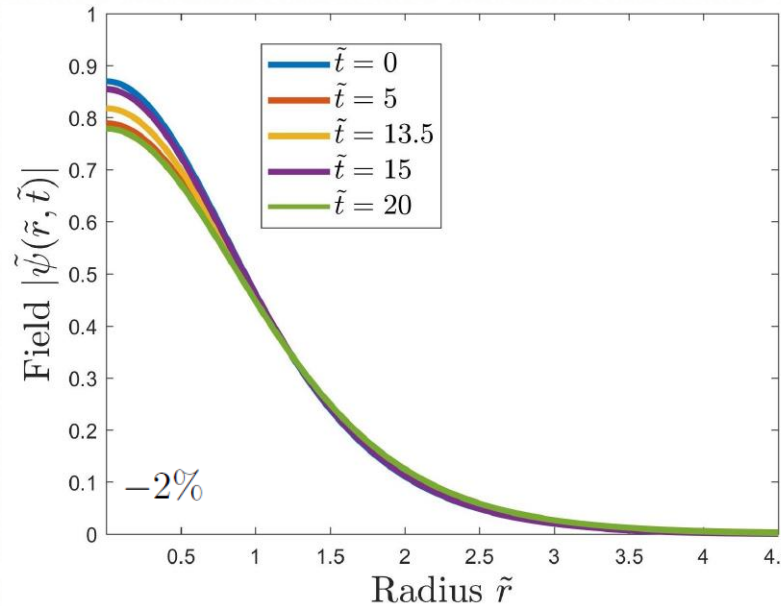
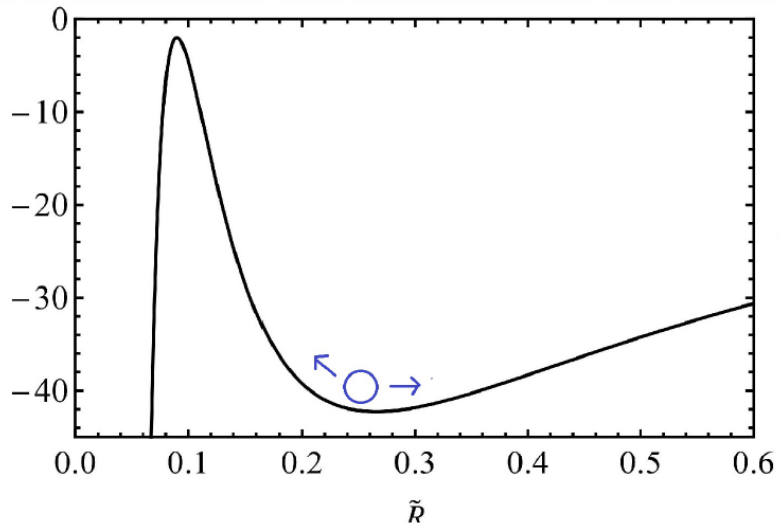
Time evolution of a clump that lives exactly on the stable branch solution .

We perturb the stable and unstable solutions as $\tilde{\psi}_{initial}(\tilde{r}) = (1 + \epsilon)\tilde{\Psi}(\tilde{r})$

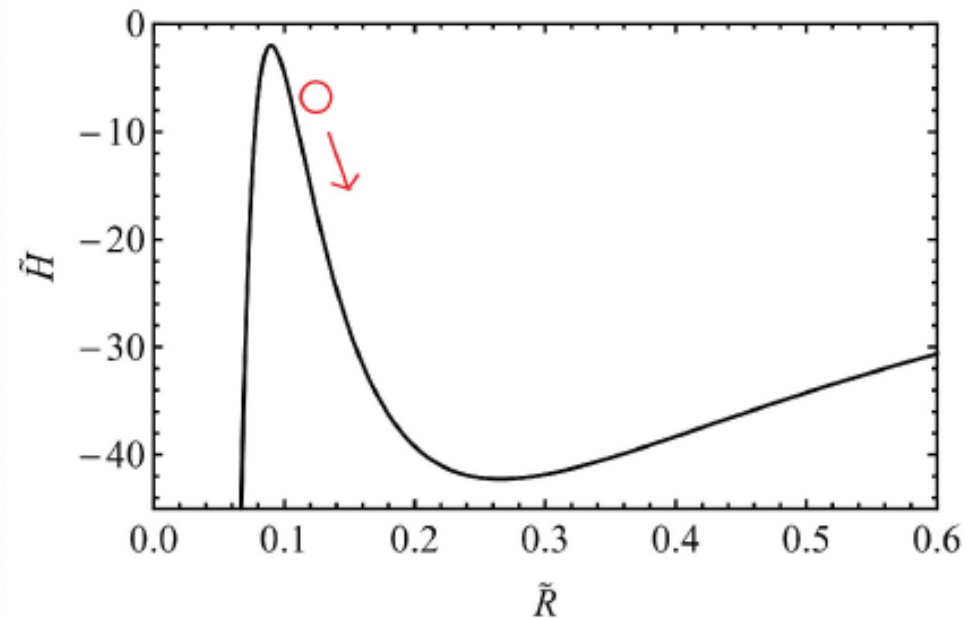
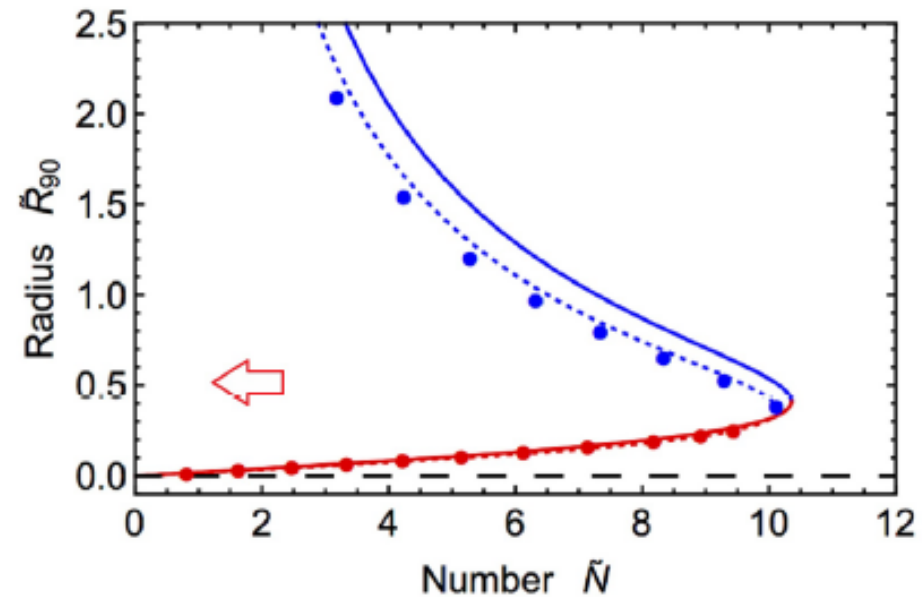
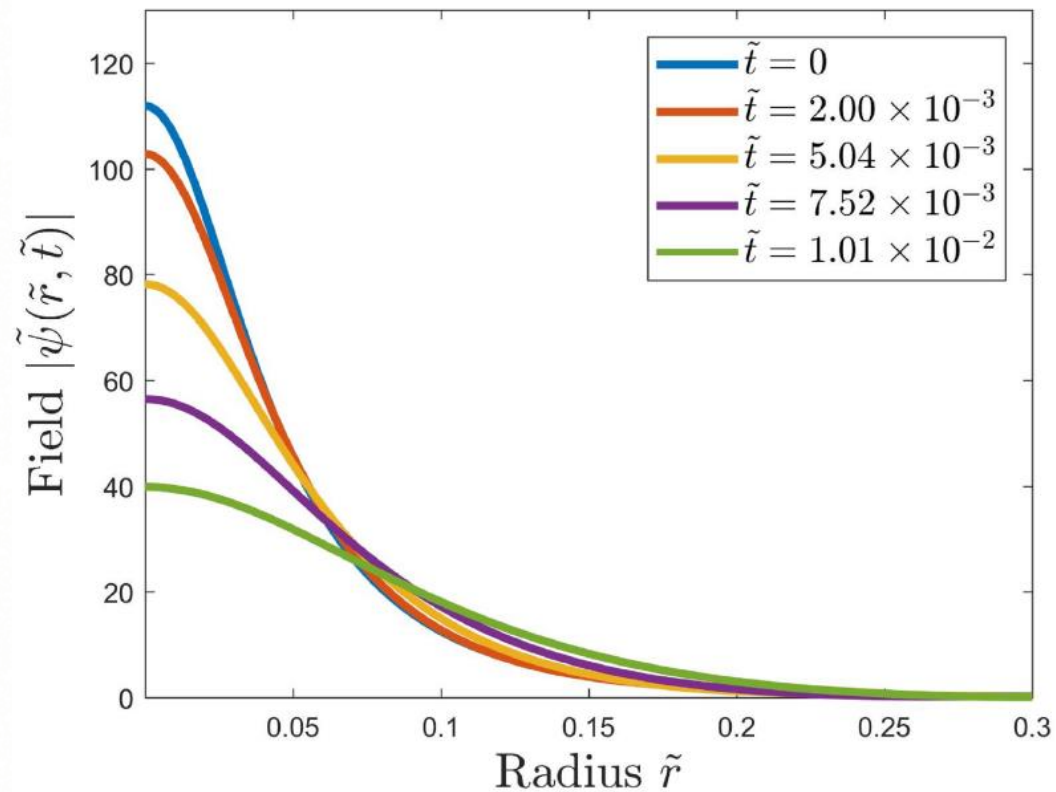
$\pm 2\%$ perturbation (Stable Branch)



(Schiappacasse and Hertzberg 2018)



-2% perturbation
(Unstable Branch)



Physical Parameters for Axion Clumps

- We compute the maximum number of particles, the maximum mass, and the minimum clump size for axion clumps as follows:

$$M_{*,max} \sim 2.4 \times 10^{19} \text{ kg} \left(\frac{10^{-5} \text{ eV}}{m_\phi} \right) \left(\frac{F_a}{6 \cdot 10^{11} \text{ GeV}} \right) \left(\frac{\gamma}{0.3} \right)^{1/2}$$

$$R_{*,min}^{90} \sim 80 \text{ km} \left(\frac{10^{-5} \text{ eV}}{m_\phi} \right) \left(\frac{6 \cdot 10^{11} \text{ GeV}}{F_a} \right) \left(\frac{0.3}{\gamma} \right)^{1/2}$$

- A simple manipulation allows us to express (M_*, R_*) of any clump as

$$M_*(R_*) = \alpha M_{*,max} (R_{*,min}^{90})$$
$$R_* = g(\alpha) R_{*,min}^{90} = \left(\frac{1 + \sqrt{1 - \alpha^2}}{\alpha} \right) R_{*,min}^{90}$$

$$\alpha \in [0, 1]$$

CLUMP CONDENSATES WITH ANGULAR MOMENTUM

- Clump condensates with non-zero angular momentum have a larger $N_{*,max}$ (and field amplitude).

$$\text{The angular momentum is } \mathbf{L} = (0,0, Nm) \text{ with } N = 4\pi \int_0^\infty dr r^2 |\Psi(r)|^2$$

- We take the field profile to be $\psi(x, t) = \sqrt{4\pi} \Psi(r) Y_{lm}(\theta, \varphi) e^{-i\mu t}$
- We look for states which minimize the energy at **fixed particle number** and **angular momentum ($l = |m|$)**
- As usual we make an ansatz for the radial profile $\Psi(r)$: For non-zero l , **the structure for small r behavior drastically changes** in comparison to the $l=0$ case

$$\text{We need } \Psi(r) = \Psi_\alpha r^l - \frac{1}{2} \Psi_\beta r^{l+2} + \dots \text{ (near region)}$$

$$\mu_{eff} \Psi \approx -\frac{1}{2m_\phi} \left(\Psi'' + \frac{2}{r} \Psi' \right) + \frac{l(l+1)}{2m_\phi r^2} \Psi \text{ (near region)}$$

MODIFIED GAUSSIAN ANSATZ

$$\Psi(r) = \sqrt{\frac{N}{2\pi(1+\frac{1}{2})!R^3}} \left(\frac{r}{R}\right)^l e^{-r^2/(2R^2)}$$

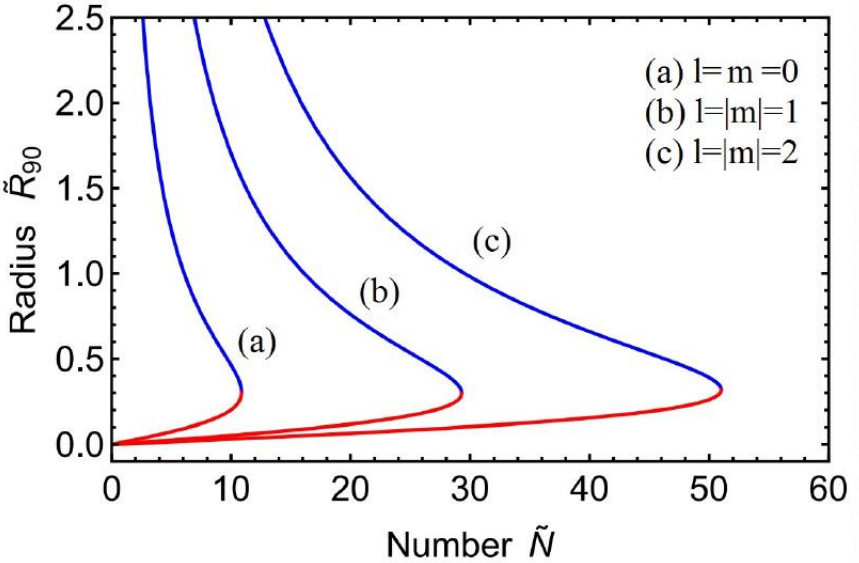
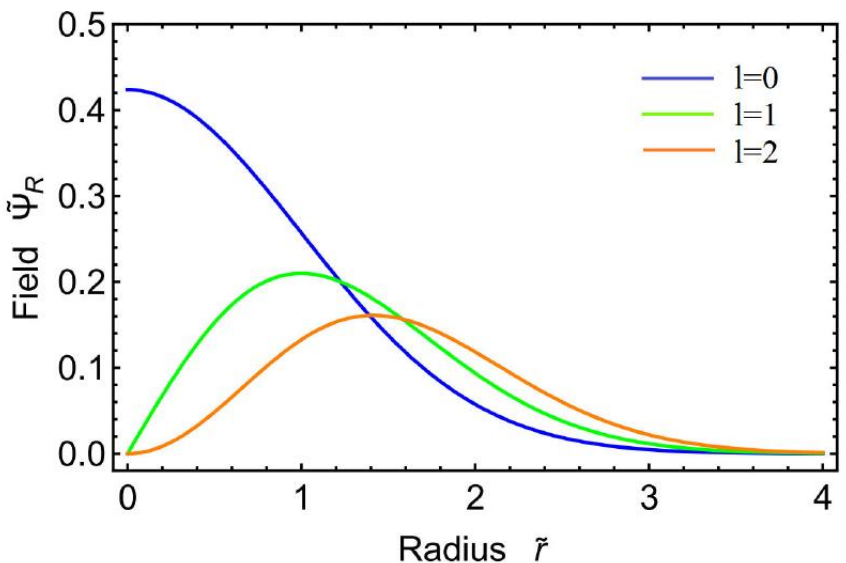
$$H(R) = a_{lm} \frac{N}{m_\phi R^2} - b_{lm} \frac{Gm_\phi^2 N^2}{R} + c_{lm} \frac{\lambda N^2}{m_\phi^2 R^3}$$

It includes the gravitational term

These terms blow up when $r \rightarrow 0$

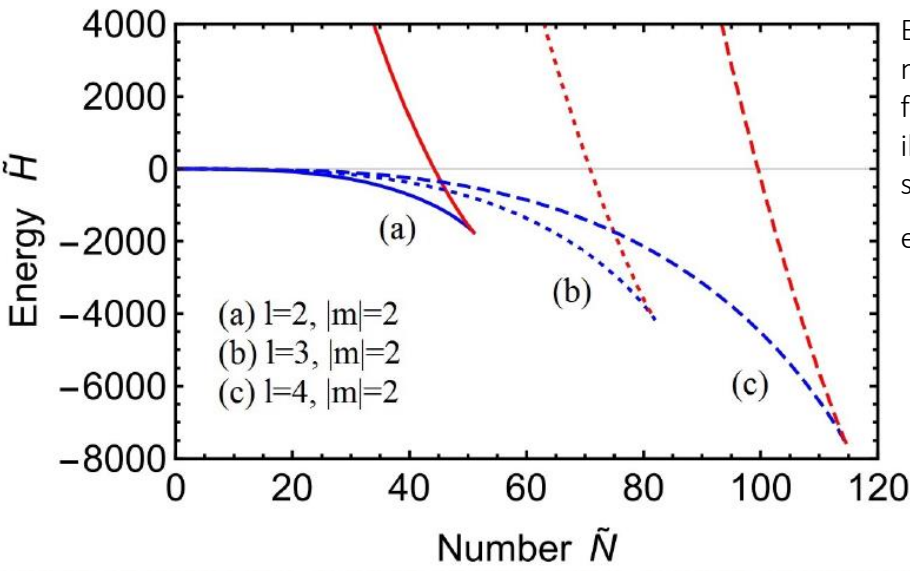
The Hamiltonian is a generalization of the previous one for the $l = 0$ case: constant coefficients (a, b, c) become $\{l, m\}$ -dependent

Field $\tilde{\Psi}_R = \Psi_R \sqrt{R^3/N_*}$ versus radius $\tilde{r} = r/R$ in the modified Gaussian ansatz for different values of spherical harmonic number l .



We plot R_{90} ($0.9N = 4\pi \int_0^{R_{90}} dr' r'^2 \Psi(r')^2$), where $\tilde{R}_{90} = m_\phi \delta^{1/2} R_{90}$ and $\tilde{N}_* = |\lambda| \delta^{1/2} N_*$.

(Hertzberg and Schiappacasse, 2018)



Energy of clump solution versus number with non-zero angular momentum parameter $|m| = 2$ for different values of l . At a fixed number N and angular momentum $L_z = Nm$, this illustrates that the configurations that minimizes the energy has spherical harmonic number $l = |m|$ (whenever the solution exists). Here $\tilde{H} = |\lambda|^3 / (m_\phi^2 \sqrt{G}) H$ and $\tilde{N}_* = m_\phi \sqrt{G} |\lambda|$.

$$\delta \equiv \frac{G_N F_a^2}{\gamma}$$

At high $l = |m|$,

$$N_{*,max} \approx \frac{10.52}{|\lambda| \sqrt{\delta}} \frac{(l^{3/2})}{(\ln l)^{1/4}} ; R_{min} \approx \frac{0.141}{m_\phi \sqrt{\delta}} \frac{(l^{1/2})}{(\ln l)^{1/4}}$$

- Lattice simulations performed by Levkov, Panin and Tkachev (2018) show **axion stars may nucleate kinetically in virialized dark matter halos**/axion miniclusters through gravitational BEC.

$$(m_a v_a) \times (R_{halo}) \gg 1$$

$$(m_a v_a^2) \times (\tau_{gr}) \gg 1$$

- The **kinetic regime** is where the field coherence length is much smaller than the characteristic scale of density variations

- The **condensation time scale** is proportional to the inverse **kinetic relaxation rate**

$$\tau_{gr} \sim 1/\Gamma_{kin} \rightarrow$$

$$\tau_{gr} \simeq \frac{4\sqrt{2}}{27\pi \Lambda} \left(\frac{R_{halo}}{v_a} \right) (R_{halo} m_a v_a)^3$$

$$\Gamma_{kin} \sim n_a \sigma_{gr} v_a \mathcal{N} \left\{ \begin{array}{l} \mathcal{N} = (6\pi^2 n_a)/(m_a v_a)^3 \\ \sigma_{gr} \approx 8\pi m_a^2 G_N^2 \Lambda / v_a^4 \\ \Lambda \equiv \log_e(m_a v_a R_{halo}) \end{array} \right.$$

Occupancy number related to Bose enhancement

Gravitational Cross Section

Coloumb logarithm

Gravitational Bose-Einstein Condensation in the Kinetic Regime

D. G. Levkov,^{1,2,*} A. G. Panin,^{1,2} and I. I. Tkachev^{1,3}

¹Institute for Nuclear Research of the Russian Academy of Sciences, Moscow 117312, Russia

²Moscow Institute of Physics and Technology, Dolgoprudny 141700, Russia

³Novosibirsk State University, Novosibirsk 630090, Russia

- The Wigner distribution f_W for ψ is shown to obey a kinetic equation sourced by the Landau scattering term $\sim f_W/\tau_{gr}$, when $\hbar(mv)^{-1} \ll R$.

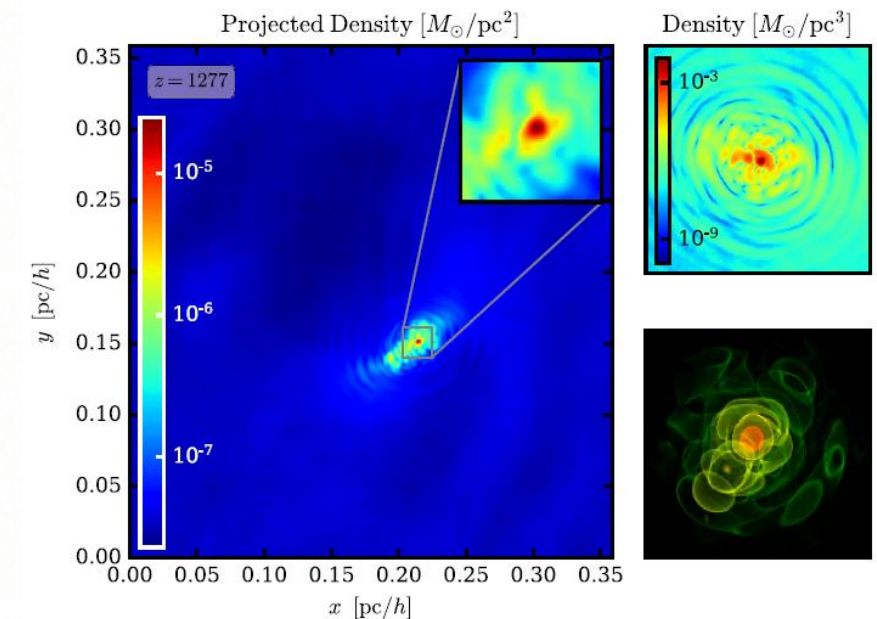
- Initial Conditions: **lattice simulations of the axion field evolution** throughout the QCD phase transition including formation of strings and domain walls.
- With their large numerical simulations it is possible to analyze the small scale structure of the axion density field and its collapse into axion miniclusters.
- Outside of the axion stars, the miniclusters consist of incoherent granular density fluctuations produced by wave interference.

The density profile of the incoherent halo decay as $r^{-9/4}$

The axion stars form roughly during **a few free-fall times** after the collapse of the minicluster.

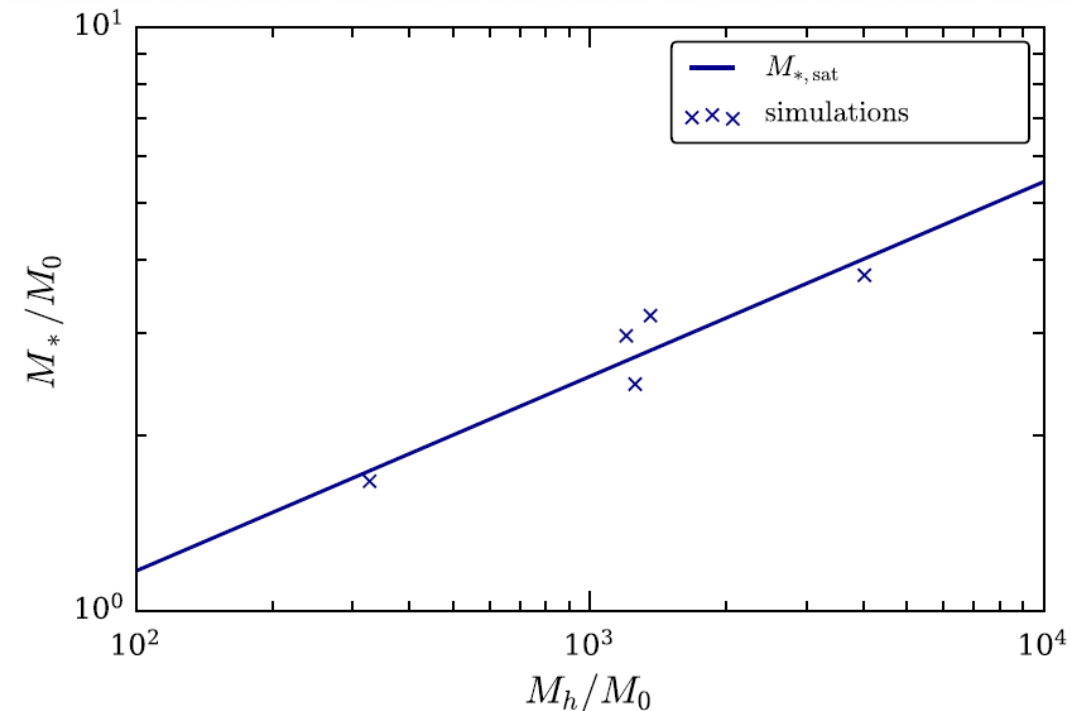
Axion stars are surrounded by pronounced **density waves**.

FIG. 1. The left panel displays the projected density of a typical simulation in comoving units. The large box shows the full simulation domain. A zoom-in of the region where the axion star has formed is shown in the inlay. The granular structure within a radius of $0.021 \text{ pc}/h$ can be more clearly seen in the slice plot in the upper right panel. A volume rendering of the axion star is shown in the lower right panel.



- After nucleation, axion star masses increase by $\sim 15\%$ with a time dependence consistent with the mass growth of Bose Stars in the kinetic regime (Levkov, Panin and Tkachev 2017)

$$\tau_{\text{gr}} \simeq \frac{4\sqrt{2}}{27\pi\Lambda} \left(\frac{R_{\text{halo}}}{v_a} \right) (R_{\text{halo}} m_a v_a)^3 \quad \rightarrow \quad M_*(t) \simeq M_{*,0} \left(\frac{t}{\tau} \right)^{1/2}$$



The saturated mass follows the core-halo mass relation $M_* \sim M_{\text{halo}}^{1/3}$

$$v_{\text{vir},*}(M_*) \simeq \frac{GM_* m}{\hbar}$$

$$v_{\text{vir,mc}}^2 = 3GM_h/10R_h$$

The saturated mass is obtained by equating the axion minicluster virial velocity with the virial velocity in the gravitational potential of the axion star

FIG. 3. Axion star masses as a function of their host halo masses, determined at the time at which a stable axion star has formed. The solid line shows the prediction from saturated mass growth in Eq. (10) consistent with the core-halo mass relation for FDM halos found in [33] with $M_0 \sim 4.4 \times 10^{-14} (m/10^{-8} \text{ eV})^{-3/2} M_\odot$.

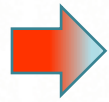
(Eggemeier and Niemeyer, 2019)

AXION STAR NUCLEATION IN DARK HALOS AROUND PBHs

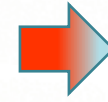
Dark minihalos

(Hertzberg, Schiappacasse, Yanagida 2020).

- Codark matter scenario:
AXIONS (mass m_a) + PBHs



PBHs behave as a cold dark matter.



$M_{\text{PBH}} > 10^{15}$ gr do not evaporate but begin to form compact dark matter halos by accreting the surrounding

(Abbott et al., 2016)


Their possible existence has been strongly revitalized since the first detection of GWs by the LIGO-Virgo collaboration

- Since PBHs are local overdensities in the DM distribution, they act as seeds for DM structure formation.
- The kinetic formation of axion stars in dark mini-halos depends on the halo energy density, axion mass and velocity
- Evolution of a DM spherical layer around a central PBH (theory of spherical gravitational collapse)

$$\tau_{gr} \sim m_a^3 v_a^6 \rho_{halo}^{-2}$$

Where the axion field coherence length is much smaller than the halo radius

(Levkov, Panin and Tkachev, 2018)


$$\frac{d^2 r}{dt^2} = -\frac{G_N(M_{\text{PBH}} + DM)}{r^2} - \frac{8\pi G_N \rho_r r}{3} + \frac{8\pi G_N \rho_\Lambda r}{3}$$

Assuming stationary and isolated PBHs, and DM background is initially in the Hubble flow, numerical calculations show PBH dark mini-halos mainly grow during the matter-dominated era reaching up to $\sim 10^2 M_{\text{PBH}}$

After the z_{eq} the mass of the dark halo surrounding PBHs grows proportionally to the cosmic scale parameter

(Mack, Ostriker and Ricotti, 2007)

$$M_{\text{halo}}(z) = 3 \left(\frac{1000}{1+z} \right) M_{\text{PBH}},$$

$$R_{\text{halo}}(z) = 0.019 \text{ pc} \left(\frac{M_{\text{halo}}}{M_{\odot}} \right)^{1/3} \left(\frac{1000}{1+z} \right).$$



$$\rho_{\text{halo}}(r) = \frac{1}{4\pi r^2} \frac{dM_{\text{halo}}(r)}{dr} \simeq 6 \times 10^{-21} \frac{\text{gr}}{\text{cm}^3} \left(\frac{\text{pc}}{r} \right)^{9/4} \left(\frac{M_{\text{PBH}}}{10^2 M_{\odot}} \right)^{3/4}$$

The efficiency of the minihalo formation will depend on **the particle-nature** of the axion DM.

$$\frac{\lambda_{\text{DB}}}{R_{\text{halo}}} \sim 6 \times 10^{-11} \left(\frac{10^{-5} \text{ eV}}{m_a} \right) \left(\frac{M_{\odot}}{M_{\text{PBH}}} \right)^{2/3} \left(\frac{1+z}{1000} \right)^{7/6}$$

These relations hold until the time of first galaxies formation at $z \sim 30$, when dressed PBHs begin to interact with non-linear structures.

- Cuspy profile with a density running with the radius as $\rho \sim r^{-9/4}$ (Bertschinger 1985)
- Such a steep profile was confirmed by N-body numerical simulations performed in Adamek 2019.

- Here $\lambda_{\text{DB}} = \frac{h}{m_a v_a}$ as the De Broglie axion wavelength with $v_a \sim (G_N M_{\text{halo}} / R_{\text{halo}})^{1/2}$

- So, we expect star nucleation mostly occurs in inner shells of PBH mini-halo at radius r_{halo} , such that $M_{halo}(r_{halo}) \gg M_{PBH}$

Levkov, Panin and Tkackev (2018) reported axion star nucleation in the center of axion miniclusters.

Eggemeier and Niemeyer (2019) reported axion star nucleation in local density maxima of axion minicluster

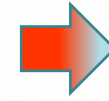
$$\frac{r_{halo}}{R_{halo}} \sim \left(\frac{k M_{PBH}}{M_{halo}} \right)^{4/3}$$

Fraction of the mini-halo radius which encloses k – *times* the central PBH mass

- Take $k \sim 10$ as an example. Since nucleation of stars occurs at $30 \lesssim z_* \lesssim 115$, we may expect nucleation occurs in spherical shells at a distance from the central PBH

$$0.05 R_{halo}(z_* \simeq 30) \lesssim r_{halo} \lesssim 0.28 R_{halo}(z_* \simeq 115)$$

- Suppose that at redshift z , the dark mini-halo satisfy conditions for axion star nucleation with $\tau_{gr}(z)$



$$\Omega_{*,0} = \left(\frac{N_* M_*}{M_{\text{PBH}}} \right) \xi_{\text{SDM}}^{\text{PBH}} \Omega_{\text{DM},0}$$

$\Omega_{*,0}$ needs to be taken as an upper bound (we are not considering disruptive events acting on axion stars after their formation)

N_* is the average number of axion stars per halo after nucleation

M_* is the characteristic mass of axion stars

- Axion stars after nucleation continue capturing axions from the halo until the growth rate slows down and saturates.
- By equating $v_a \sim (G_N M_{\text{halo}} / R_{\text{halo}})^{1/2}$ to the virial velocity in axion star potential:

$$\left(\frac{M_*}{M_0} \right) \simeq (1 + z_*)^{1/2} \left(\frac{M_{\text{halo}}}{M_0} \right)^{1/3} \Rightarrow M_* \sim (M_{\text{PBH}}^{1/2} \overline{M}_0)^{2/3} \quad \text{where} \quad \overline{M}_0 = \sqrt{3000} M_0$$

Up to a numerical factor of order one, the same scaling relation was found for solitonic cores in halos of fuzzy DM

$$M_0 \simeq 5.5 \times 10^{-19} M_{\odot} (10^{-5} \text{ eV}/m_a)^{3/2}$$

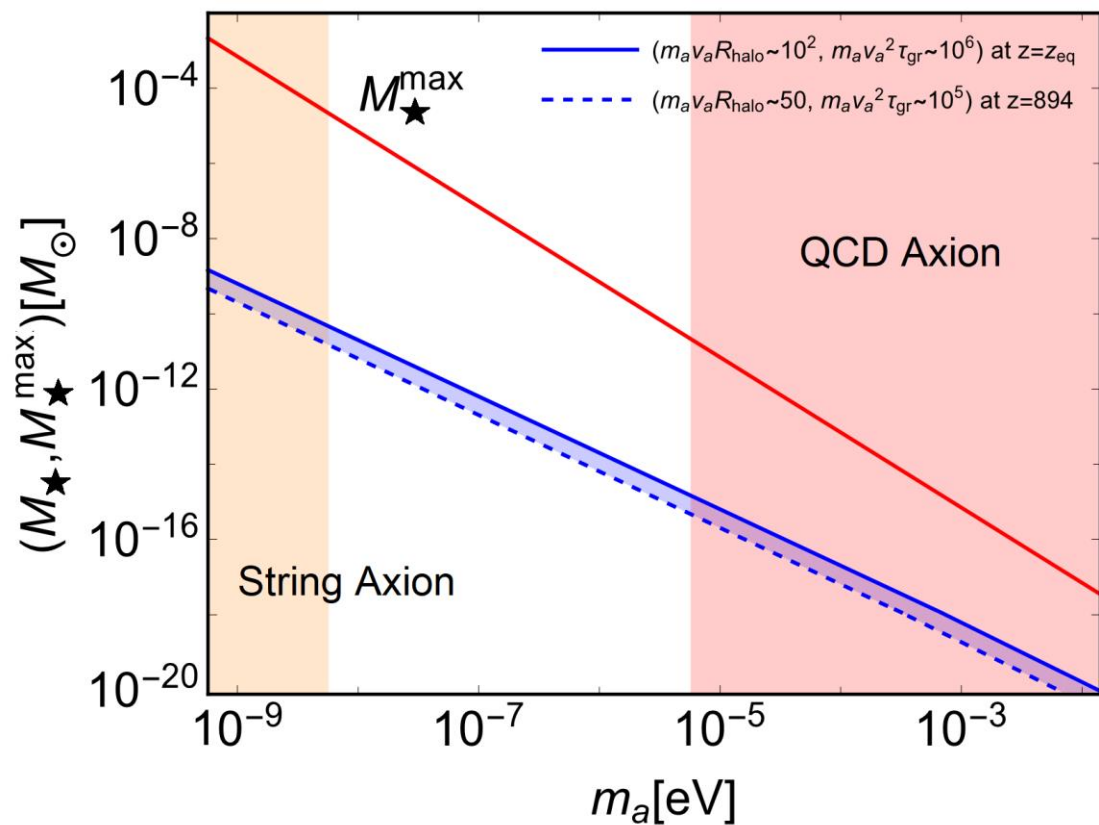


FIG. 2. Contour-levels of $(m_a v_a R_{\text{halo}}, m_a v_a^2 \tau_{\text{gr}})$ in the parameter space (m_a, M_*) . The blue shaded region between the blue solid ($z = z_{\text{eq}}$) and dashed ($z = 894$) lines corresponds to the parameter space of (m_a, M_*) at which the kinetic regime is satisfied as $(m_a v_a R_{\text{halo}}, m_a v_a^2 \tau_{\text{gr}}) \gtrsim (50, 10^5)$ at $894 < z < z_{\text{eq}}$. Red (orange) band corresponds to the mass range for the QCD (string) axion. The red solid line indicates the theoretical maximum mass, M_*^{\max} , that an axion star in the ground state configuration can achieve [23].

Values for M_* are far away to reach or overpasses the maximum mass allowed for a stable axion star configuration

$$M_*^{\max} \sim 7 \times 10^{-12} M_\odot (10^{-5} \text{ eV}/m_a)^2$$

QCD axion $\mathcal{O}(10^{-20}) M_\odot \lesssim M_* \lesssim \mathcal{O}(10^{-15}) M_\odot$

string axion $\mathcal{O}(10^{-11}) M_\odot \lesssim M_* \lesssim \mathcal{O}(10^{-9}) M_\odot$

Collapse and explosion in relativistic axions is unlikely

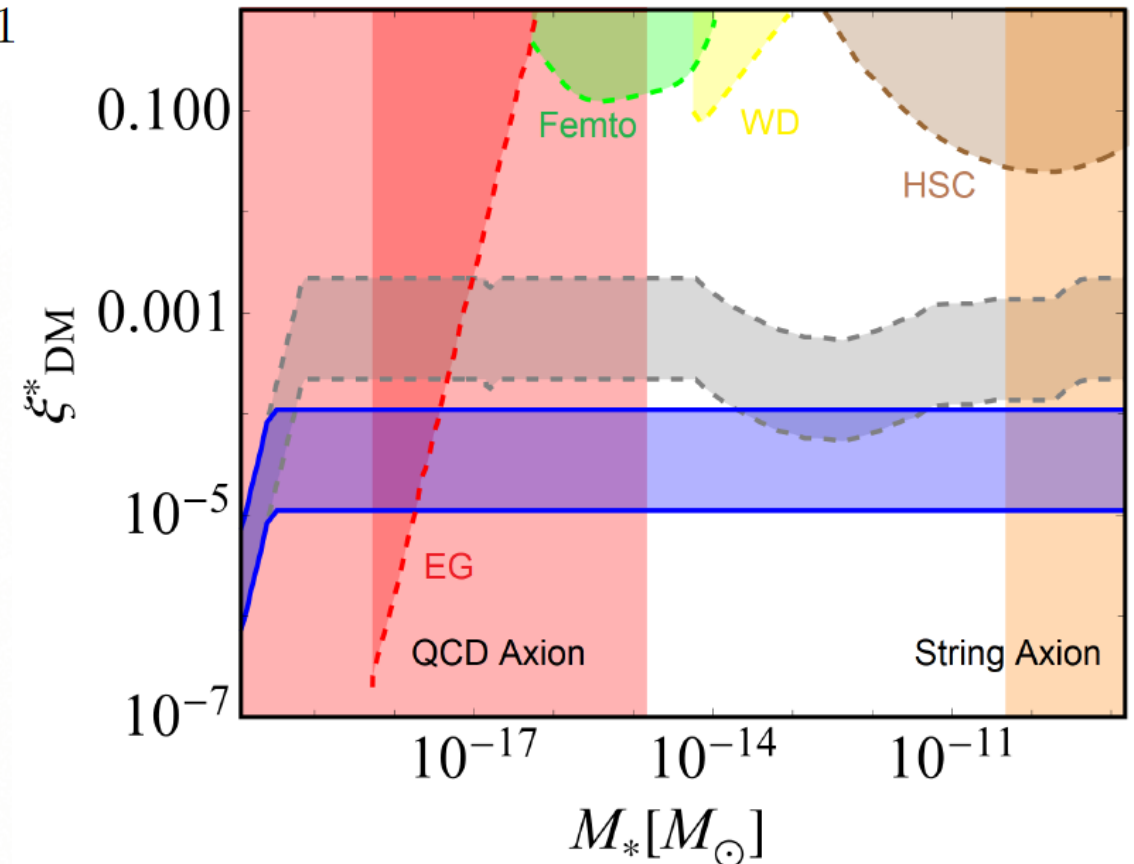
(Levkov, Panin and Tkachev 2017)

- Thus, we may express the current parameter density for axion stars in function of the PBH and axion masses as

$$\Omega_{\star,0} \sim N_{\star} \left(\frac{\overline{M_0}}{M_{\text{PBH}}} \right)^{2/3} \xi_{\text{DM}}^{\text{PBH}} \Omega_{\text{DM},0} \quad \text{where } N_{\star} \geq 1$$

$$\xi_{\text{DM}}^{\text{PBH}} = \min(\xi_{\text{DM,max}}^{\text{PBH}}, Q)$$

The blue (gray) shaded band shows the estimate of the current fraction of dark matter in axion stars ξ_{DM}^{\star} by using Eq. (24), a fraction in PBHs no greater than 0.5% (10%), $1 \leq N_{\star} \leq 10$, and the contour-level $(m_a v_a R_{\text{halo}}, m_a v_a^2 \tau_{\text{gr}}) \sim (10^2, 10^6)$ at $z = z_{\text{eq}}$ in the parameter space $(M_{\text{PBH}}, M_{\star})$. Light red (light brown) band corresponds to the mass range of axion stars associated with the QCD (string) axion. In addition, we have shown constraints over the PBH abundance. In particular, extragalactic photon background (EG), femtolensing (Femto), white dwarfs in our local galaxy (WD), and Subaru HSC data (HSC).



(Hertzberg, Schiappacasse, Yanagida 2020)

Fate of Axion Stars

- Suppose conditions in dark mini-halos for formation of axion stars are satisfied such that they are formed before first galaxies formation.

- Tidal forces coming from the mean field potential of the dressed PBH will try to disrupt axion stars after formation

$$r_{\text{tidal}} = \left(\frac{M_{\star}}{3M_{\text{PBH}_d}(R_0)} \right)^{1/3} [f_{\text{PBH}_d}(R_0)]^{-1/3} R_0,$$

We may apply the distant tide approximation so long $r_{\text{tidal}} \ll r$

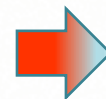
- Take a typical QCD axion star with $M_{\star} \sim 10^{-18} M_{\odot}$ and $R_{\star} \sim 2 \times 10^{-9} \text{pc}$ which was nucleated within a dressed PBH with $M_{\text{PBH}} \sim 2 \times 10^{-16} M_{\odot}$, $M_{\text{halo}} \sim 6 \times 10^{-15} M_{\odot}$ and $R_{\text{halo}} \sim 3 \times 10^{-6} \text{pc}$.

- Some axion stars may **leave mini-halos**
- Some axion stars may **remain within mini-halos**.
- An eventual merger** between axion stars and the central PBH is also possible

with $f_{\text{PBH}_d}(R_0) = 1 - \frac{1}{3} \frac{d \ln M_{\text{PBH}_d}(r)}{d \ln r} \Big|_{R_0}$

$$M_{\text{PBH}_d}(r) = 4\pi \int_{r_{\text{min}}}^r dr r^2 \rho_{\text{halo}}(r) + M_{\text{PBH}}$$

Mass of the dressed PBH inside the radius r



$$r_{\text{tidal}}/R_{\star} \simeq 30 \text{ at } R_0 \sim 0.28 R_{\text{halo}}$$

- The likelihood of a merger between the nucleated axion star and the PBH may be estimated by calculating the free-fall time

$$t_{\text{ff}} \sim (\pi/2) R_0^{3/2} / \sqrt{2G_N(M_{\text{PBH}})} \quad \text{where } M_{\text{PBH}} \gg M_\star$$

For a typical QCD axion star, we have $t_{\text{ff}} \sim \text{Myr}$, which is a long time.

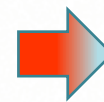
- In any case, we expect galactic halos at the time of formation around $z \sim 6$ would be composed by

- Isolated and clustered dressed PBHs (with axion stars)
- Naked PBHs
- Axion stars
- Smooth axion dark matter background

- The total local number of axion stars can be expressed as

$$N_{\star, \text{local}}^{\text{total}} \simeq 10^{11} \left(\frac{\xi_{\text{DM}}^*}{0.03} \right) \left(\frac{10^{-11} M_\odot}{M_\star} \right) \left(\frac{r}{100 \text{ pc}} \right)^3$$

Taking a 0.5% in the fraction of DM in axion stars, we have for a typical QCD (string) axion stars $\sim 10^{17} (10^9)$ axion stars around our Sun in a radius of 100 PC



if a non-negligible number of axion stars survive tidal disruptions, then their presence today within the Milky Way halo would enhance DM indirect detection experiments.

Near Field Region

- The time independent field equation for a spherically symmetric eigenstate is

$$\mu\Psi = -\frac{1}{2m}\left(\Psi'' + \frac{2}{r}\Psi'\right) - 4\pi G_N m^2 \Psi \int_0^\infty dr' r'^2 \frac{\Psi(r')^2}{r_>} + \frac{1}{2} \frac{\partial V_{nr}}{\partial \Psi}$$

- We may replace $r_>$ by r' in the gravitational term and then move the integral to the right to define

$$\mu_{eff} = \mu + 4\pi G m^2 \int_0^\infty dr' r' \Psi(r')^2$$

- By now, just let me drop the self-interacting term to obtain:

$$\mu_{eff} \Psi \approx -\frac{1}{2m}\left(\Psi'' + \frac{2}{r}\Psi'\right) \quad (\text{near region, ignoring } V_{nr})$$

Here the chemical potential is positive and solutions are spherical Bessel functions.

$$\Psi(r) \propto j_0(\sqrt{2m\mu_{eff}} r) = \frac{\sin(\sqrt{2m\mu_{eff}} r)}{\sqrt{2m\mu_{eff}} r} \quad (\text{near region, ignoring } V_{nr})$$

Including self-interactions the shape is corrected but the salient feature that survives is that the solution is an inverted parabola centered at $r = 0$, plus higher order corrections

$$\Psi(r) = \Psi_0 - \frac{1}{2}\Psi_2 r^2 + \dots \quad (\text{near region})$$

SPHERICALLY SYMMETRIC CLUMP CONDENSATES

Black Holes Formation

- The ground state is well described by the weak field gravitational approximation:

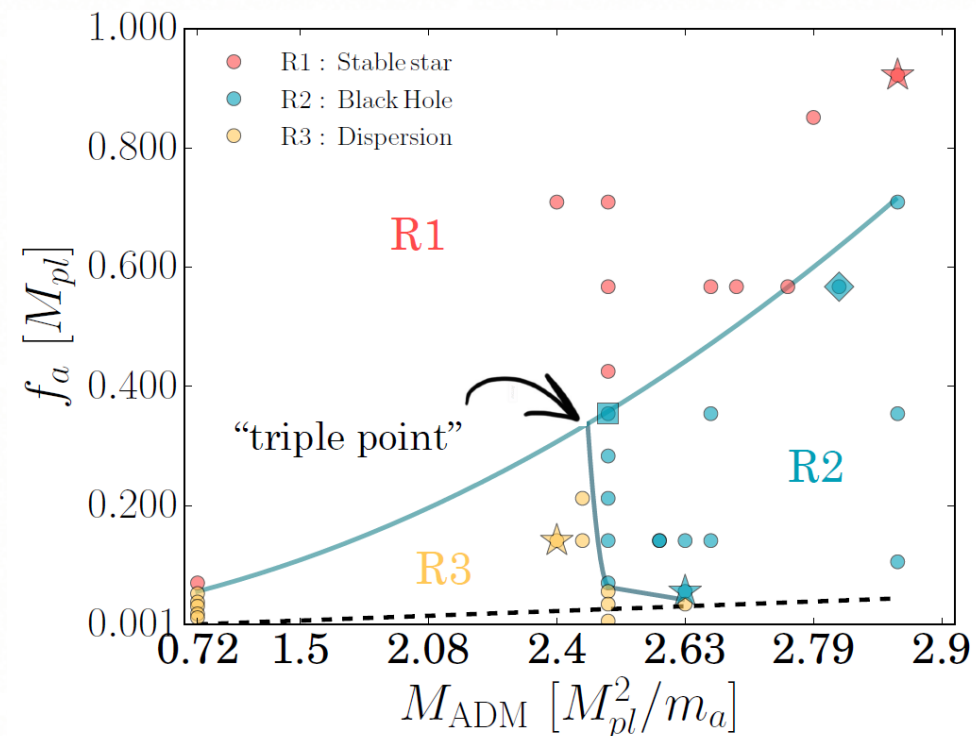
$$\frac{R}{R_S} > \frac{R_{min}}{2G_N M_{max}} \approx 4 \times 10^{12} \left(\frac{6 \times 10^{11} \text{ GeV}}{F_a} \right)^2 \quad \rightarrow$$

So there is no possibility of black hole formation of these low-density objects when $F_a \ll M_{pl}$.

(Helfer et al., 2017)

- Strong fields effects can emerge if one were to move away from the traditional QCD axion and investigate extremely high values of F_a .

Collapsing axion stars by using full non-linear Einstein equations of general relativity and the full non-perturbative cosine potential



DENSE BRANCH AND AXITONS

- We need ($\omega \approx m$) to trust non-relativistic approximations ($\phi \ll f_a$). For the stable branch this condition is always satisfied. For the unstable branch this condition is broken when $\tilde{N} \lesssim \vartheta(10^{-5})$ for the QCD axion.

- We drop gravitational corrections and take an approximate periodic clumps solution as $\phi(r, t) = \Phi(r)\cos(\omega t)$

- We insert this into the relativistic Hamiltonian (ignoring gravity but including the full cosine potential) and average over a period of oscillation $T = 2\pi/\omega$ as $\langle H \rangle = \frac{1}{T} \int_0^T dt H$

$$\langle H \rangle = 4\pi \int_0^\infty dr r^2 \left[\frac{\omega^2}{4} \Phi^2 + \frac{1}{4} \Phi'^2 + m^2 f_a^2 [1 - J_0(\Phi/f_a)] \right]$$

- To specify the condition

for ω , we take the time average of $\ddot{\phi} - \nabla^2 \phi + m^2 f_a \sin(\phi/f_a) = 0$

equation of motion and integrate over space.

$$\Rightarrow \omega^2 \approx 2m^2 \left[\int_0^\infty dr r^2 J_1(\Phi/f_a) \right] / \left[\int_0^\infty dr r^2 (\Phi/f_a) \right]$$

- We use an exponential ansatz for the radial profile:
 $\Phi(r) = 2\pi\epsilon f_a e^{-r/R}$, where $0 < \epsilon < 1 \mapsto |\phi| < 2\pi f_a$

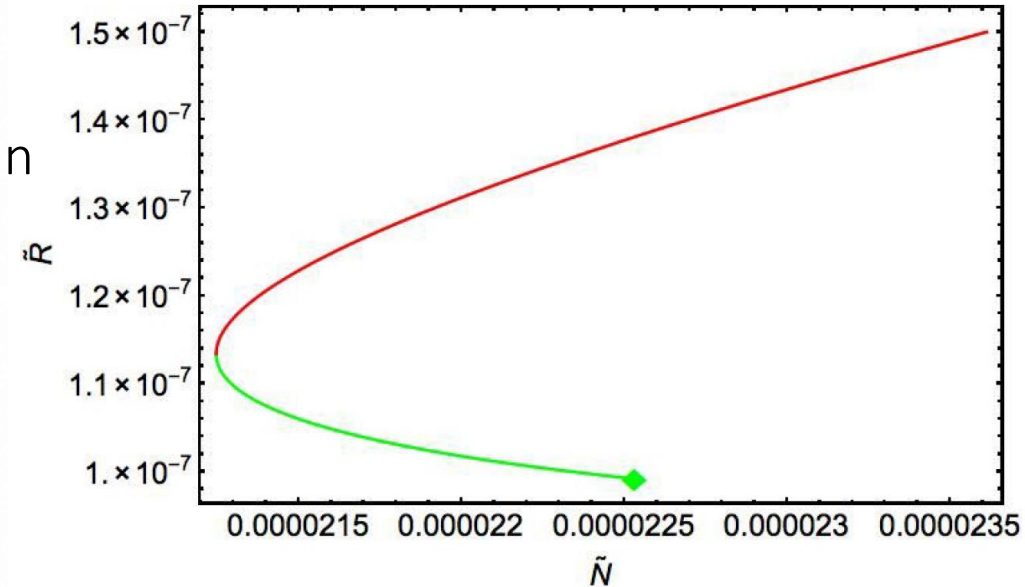
- We expand the Bessel function to evaluate the Hamiltonian
 With the exponential profile to find

$$\langle H \rangle = f_a^2 \pi^3 R \epsilon^2 (1 + m^2 R^2 g(\epsilon))$$

Generalized Hypergeometric functions

- We extremize $\langle H \rangle$ at a “fixed” number of particles by
 using $\langle N \rangle = \int d^3x \omega \langle \phi^2 \rangle$

(Schiappacasse and Hertzberg, 2018)



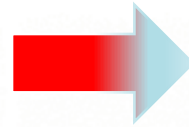
- Axions:** relativistic solutions with frequencies of oscillations far from m (Kolb & Tkachev, 1993)
- Such solutions are quasistable since they radiate relativistic axions at an appreciable rate.

- The number of encounters between the Earth and an axion star per unit of time is calculated as

$$N_{\otimes \star} = n_{\star,0}^{\text{local}} \sigma_{\text{eff}} v_{\text{rel}} \quad \text{where } n_{\star,0}^{\text{local}} = \xi_{\text{DM}}^* \rho_{\text{DM,local}} / M_{\star}$$

$$M_{\star} \sim 10^{-18} M_{\odot} \quad \text{QCD axion}$$

$$M_{\star} \sim 10^{-10} M_{\odot} \quad \text{string axion}$$



$$N_{\otimes \star} \sim 10^{-1} \text{ Myr}^{-1}$$

$$N_{\otimes \star} \sim 10^{-3} \text{ Myr}^{-1}$$

Taking a conservative 0.5% of DM in axion stars and $v_{\text{rel}} \sim 3 \times 10^2 \text{ km/s}$, chances of direct detection of DM by the Earth passing through an axion star is **extremely small**.